Cellular and Molecular Life Sciences
https://doi.org/10.1007/s00018-019-03130-4

Cellular and Molecular Life Sciences

ORIGINAL ARTICLE

Listeria monocytogenes hijacks CD147 to ensure proper membrane protrusion formation and efficient bacterial dissemination

Aaron S. Dhanda[1] · Katarina T. Lulic[1] · Connie Yu[1] · Robert H. Chiu[2,3] · Michael Bukrinsky[4] · Julian A. Guttman[1]

Received: 3 January 2019 / Revised: 12 April 2019 / Accepted: 2 May 2019

Abstract

Efficient cell-to-cell transfer of *Listeria monocytogenes (L. monocytogenes)* requires the proper formation of actin-rich membrane protrusions. To date, only the host proteins ezrin, the binding partner of ezrin, CD44, as well as cyclophilin A (CypA) have been identified as crucial components for *L. monocytogenes* membrane protrusion stabilization and, thus, efficient cell-to-cell movement of the microbes. Here, we examine the classical binding partner of CypA, CD147, and find that this membrane protein is also hijacked by the bacteria for their cellular dissemination. CD147 is enriched at the plasma membrane surrounding the membrane protrusions as well as the resulting invaginations generated in neighboring cells. In cells depleted of CD147, these actin-rich structures appear similar to those generated in CypA depleted cells as they are significantly shorter and more contorted as compared to their straighter counterparts formed in wild-type control cells. The presence of malformed membrane protrusions hampers the ability of *L. monocytogenes* to efficiently disseminate from CD147-depleted cells. Our findings uncover another important host protein needed for *L. monocytogenes* membrane protrusion formation and efficient microbial dissemination.

Keywords Comet/rocket tails · Cell-to-cell spreading · Actin-based motility · Infectious disease · Microbiology · Actin

Introduction

Listeria monocytogenes (*L. monocytogenes)* is an invasive food-borne bacterial pathogen that is the causative agent of listeriosis; an infection with 20–30% mortality rates [1].

The strategies used by *L. monocytogenes* to cause disease often arise from the microbes hijacking their host's subcellular machinery [2]. The host actin cytoskeleton is a crucial target for *L. monocytogenes* and is controlled during their invasion into and movement within (and amongst) host cells [2–5]. Movement within the cytoplasm of their host cells is accomplished through their generation of actin-rich structures called comet/rocket tails [2, 6]. During comet/rocket tail formation, the N-WASp mimicking bacterial surface protein ActA binds to and activates the Arp2/3 complex where branched actin filaments (F-actin) provide the propulsive force necessary for motility [7]. Movement of *L. monocytogenes* amongst host cells occurs when motile bacteria engage the host cell periphery resulting in the formation of modified comet/rocket tails that protrude from the cell and are sheathed by plasma membrane [2]. These actin-rich membrane protrusions interact with corresponding invaginations in neighboring cells which ultimately enable *L. monocytogenes* to spread from one cell to another.

We have recently shown that the eukaryotic prolyl *cis–trans* isomerase, cyclophilin A (CypA), is hijacked by *L. monocytogenes* exclusively at membrane protrusions [8]. CypA is essential for their structural integrity, as cells

Electronic supplementary material The online version of this article (https://doi.org/10.1007/s00018-019-03130-4) contains supplementary material, which is available to authorized users.

✉ Julian A. Guttman
jguttman@sfu.ca

[1] Department of Biological Sciences, Centre for Cell Biology, Development, and Disease, Simon Fraser University, Burnaby, BC, Canada

[2] Dental and Craniofacial Research Institute and School of Dentistry, University of California, Los Angeles, Los Angeles, CA, USA

[3] Surgical Oncology and Jonsson Comprehensive Cancer Center, University of California, Los Angeles, Los Angeles, CA, USA

[4] The George Washington University School of Medicine and Health Sciences, 2300 Eye St NW, Washington, DC 20037, USA

depleted of CypA form membrane protrusions that are morphologically deformed [8]. Importantly, malformed membrane protrusions cause a reduction in *L. monocytogenes* cell-to-cell spreading. This uncommon phenotype is also observed with inhibition of the ERM family protein ezrin and its binding partner CD44 [9].

To further tease out cellular components involved in the formation of *L. monocytogenes* membrane protrusions, we set out to examine known CypA-binding partners that associate with both the plasma membrane and the actin cytoskeleton. We identified the eukaryotic plasma membrane protein CD147; a well-known binding partner of secreted CypA, as a candidate to study during *L. monocytogenes* infections [10]. CD147 expression promotes proper cytoskeletal organization [11] as well as focal adhesion [12], lamellipodium [12–14], and invadopodium [15] formation in vitro. Recent evidence also highlights a unique cytoskeletal-associated role of CD147 in organizing protrusive actin-rich structures generated during *Neisseria meningitidis* (*N. meningitidis*) infections of endothelial cells [16]. Here, we demonstrate that CD147 is a key host cell membrane protein that influences the cell-to-cell transfer of *L. monocytogenes*.

Methods

Cell culture

Human cervical (HeLa), lung (A549), and intestinal (Caco-2) epithelial cells were acquired from American Type Culture Collection (ATCC) (catalog numbers CCL-2, CCL-185 and HTB-37). CypA KO (PPIA-/-) mouse embryonic fibroblast cells (MEFs) [17] and HeLa cells were cultured using Dulbecco's modified Eagle's medium (DMEM) containing high glucose (Hyclone, GE Healthcare) supplemented with 10% fetal bovine serum (FBS) (Gibco, Thermo Fisher Scientific). A549 cells were cultured using Ham's F-12K (Kaighns's) medium (Gibco, Thermo Fisher Scientific) supplemented with 10% FBS. Caco-2 cells were cultured using Dulbecco's modified Eagle's medium (DMEM)-containing high glucose (Hyclone, GE Healthcare) supplemented with 10% fetal bovine serum (FBS) (Gibco, Thermo Fisher Scientific) and 1% non-essential amino acids (Hyclone, GE Healthcare). SKOV3 cells (ATCC catalog number HTB-77) were cultured using DMEM: nutrient mixture F-12 (DMEM/F-12) (Gibco, Thermo Fisher) supplemented with 10% FBS. All cell lines were maintained in a cell culture incubator (37 °C, 5% CO_2). To seed cells for experiments, cells growing in plastic culture flasks were first rinsed 3X with Dulbecco's phosphate-buffered saline without Ca^{2+} and Mg^{2+} (PBS [-/-]) (Gibco, Thermo Fisher Scientific), trypsinized with 0.05% Trypsin–EDTA (Gibco, Thermo Fisher Scientific) and then seeded onto clear polystyrene 6-well or 24-well format plates (Corning) containing glass coverslips.

Bacterial strains and growth conditions

The bacterial strains used were *L. monocytogenes* strains EGD BUG 600 (wild-type and Δ*actA*) (gifted by Dr. Pascale Cossart) and *S. flexneri* (serotype 5a strain M90T). *L. monocytogenes* bacteria were grown at 37 °C using brain heart infusion (BHI) agar or broth (BD Biosciences). *S. flexneri* bacteria were grown initially on LB agar (LBA, BD Biosciences) containing 0.01% Congo red (Ricca Chemical Company) at 37 °C to obtain red-colored colonies (indicative of virulent bacteria). Red-colored *S. flexneri* colonies were subcultured using LB broth (BD Biosciences).

Listeria monocytogenes infections

To infect cultured cells, overnight shaken-broth cultures of *L. monocytogenes* were diluted 10× in BHI broth (final volume of 10 mL) and then incubated at 37 °C in a shaking incubator (on an angle) until A600 = 1.00. At A600 = 1.00, 1 mL of bacteria were spun down for 5 min at 10,000 rpm (25 °C) and washed 2× with pre-warmed (37 °C) PBS [-/-]. Pelleted bacteria were re-suspended with 1 mL of pre-warmed serum-free media (DMEM, Kaighns's or DMEM/F-12; 37 °C) and then diluted 100×. Diluted bacteria were added onto culture plates containing host cells and incubated for at least 6–7 h to study comet/rocket tail and actin-rich membrane protrusion/invagination formation.

Shigella flexneri infections

To infect cultured cells, a single red colony (grown on LBA + 0.01% Congo red) was inoculated into 2 mL of LB broth for 18 h at 37 °C (with shaking). 18 h cultures were diluted 50-fold into 5 mL of LB broth and shaken for an additional 2 h at 37 °C. For intercellular spreading assays, optical density readings were performed following the 2 h subcultures, such that all replicate experiments were performed with bacteria grown to the same optical density. Bacteria were then added onto culture plates containing host cells and incubated at 37 °C for 1 h. After 1 h, cells were rinsed 5X with pre-warmed sterile PBS [-/-] and then left in media-containing gentamicin (50 µg/mL). Infections were fixed between 2.5 and 3.5 h to examine membrane protrusions.

Reagents and antibodies

Antibodies and reagents used in this study included: Alexa Fluor 594-, 488-, and 350-conjugated phalloidin (Invitrogen); Alexa Fluor 594-, 488-, and 350-conjugated goat

anti-rabbit and goat anti-mouse antibodies (2 µg/mL, Invitrogen); mouse anti-CD147 (10 µg/mL for immunofluorescence, Abcam, ab666); rabbit anti-cyclophilin A (10 µg/mL for immunofluorescence, Abcam, ab41684); rabbit anti-α-actinin 4 (10 µg/mL for immunofluorescence, Abcam, ab108198); mouse anti-ezrin (1:100 for immunofluorescence, Developmental Studies Hybridoma Bank, CPTC-Ezrin-1); mouse anti-α-tubulin (1:1000 for Western blot, Developmental Studies Hybridoma Bank, 12G10); rabbit anti-*Listeria monocytogenes* (1:300 for immunofluorescence, BD Difco, 223021); rabbit anti-*Shigella flexneri* (1:50 for immunofluorescence, BD Difco, BD 228351); normal mouse IgG (10 µg/mL for immunofluorescence, Invitrogen, Thermo Fisher Scientific); HRP-conjugated goat anti-mouse antibodies (1 µg/mL, Invitrogen). The mouse monoclonal anti-α-tubulin antibody (12G10) was deposited to the DSHB by Frankel J/Nelsen EM. The mouse monoclonal anti-ezrin antibody 120 (CPTC-Ezrin-1) was deposited to the DSHB by Clinical Proteomics Technologies for Cancer.

Immunolocalization

For immunofluorescence studies, cells attached to glass coverslips were fixed in the dark at room temperature for 15 min using pre-warmed (37 °C) 3% paraformaldehyde (prepared in 150 mM NaCl, 4 mM Na/K PO4, 5.0 mM KCl, and pH 7.3) and then rinsed 3× with PBS [-/-]. Cells were permeabilized at room temperate for 5 min using 0.2% Triton X-100 (prepared in PBS [-/-] and used at room temperature) or at − 20 °C for 10 min while submerged in a − 20 °C acetone bath. Following Triton X-100 treatment, coverslips were rinsed 3× with PBS [-/-], whereas acetone-treated coverslips were left to dry at room temperature for 30 min. All samples were then blocked at room temperature with 5% normal goat serum (prepared in PBS [-/-]) for 20 min after which samples were incubated overnight at 4 °C with primary antibodies prepared in TPBS/BSA (PBS [-/-], 0.5% Tween-20, 0.1% bovine serum albumin [BSA]). Following this, samples were washed 3× with TPBS/BSA for 10 min and then treated with secondary antibodies (Alexa Fluor 594- or 488-conjugated goat anti-rabbit or goat anti-mouse; prepared in TPBS/BSA) at room temperature in the dark for 2 h. To visualize F-actin, samples were incubated with Alexa Fluor 594-, 488-, or 350-conjugated phalloidin (prepared in PBS [-/-]) for 20 min. Samples were washed 3× with PBS [-/-] and mounted onto glass microscope slides using the Prolong Diamond antifade mounting medium either with or without DAPI (Invitrogen, Thermo Fisher Scientific). We considered a protein "enriched" at a specific area if the observed staining signal intensity was higher at that site (or at that structure) when compared to other regions of the cell in general and was also absent in controls.

Lysate preparation and Western blotting

Lysates were prepared by washing cells in culture well plates 3X with pre-warmed PBS [+/+] and then treating with ice-chilled RIPA lysis buffer (150 mM NaCl, 50 mM Tris, pH 7.4, 5 mM EDTA, 1% Nonidet P-40, 1% deoxycholic acid, 10% SDS) containing a cOmplete™ Mini EDTA-free protease inhibitor cocktail (Roche) on ice for 5 min. Cells were disrupted using cell scrapers and lysates collected into microcentrifuge tubes. Lysates were spun at 4 °C and 10,000 g for 10 min to pellet cellular debris and DNA; supernatants were collected into new pre-chilled microcentrifuge tubes and immediately stored at − 80 °C. Protein concentrations were determined using a bicinchoninic acid (BCA) assay kit (Pierce). For Western blotting, lysates samples were first prepared in 6× Laemmli buffer and then boiled (100 °C) for 10 min. Equal amounts of protein were loaded onto 10% SDS–polyacrylamide gels and resolved by electrophoresis. Following protein separation, gels were rinsed in water for 5 min and then transferred onto nitrocellulose membranes using a Trans-Blot® SD semi-dry transfer cell (Bio-Rad). After the transfer, the membranes were washed for 5 min in TBST (Tris-buffered saline, 0.05% Tween-20) with shaking, blocked with shaking for 1 h with 4% Blotto (Santa Cruz Biotechnology) prepared in TBST, and then treated with primary antibodies (diluted in TBST, 1% BSA) overnight at 4 °C. The next day, membranes were rinsed 3× with TBST for 10 min each prior to incubating with secondary antibodies (HRP-conjugated goat anti-rabbit or goat anti-mouse) for 1 h at room temperature. Membranes were treated with Western Lightning Plus-ECL (PerkinElmer) following the manufacturer's instructions and protein bands were visualized using a Fujifilm LAS-4000 imager (Fujifilm). To confirm equal loading, membranes were stripped of bound antibodies with mild stripping buffer (1.5% glycine, 0.1% SDS, 1% Tween-20, pH 2.2) and re-probed using the mouse anti-α tubulin targeting antibody.

DNA constructs

DNA plasmids encoding GFP-CD147, GFP-CD147-P211A, and the respective empty GFP vectors were generated previously [18, 19]. The DNA plasmid encoding pmKate2-f-mem (cat no. FP186) was purchased from Evrogen.

CD147 RNAi knockdown

A smart pool (ON-Targetplus siRNA) of 4 CD147 siRNA (L-010737-00-0005) and 4 non-targeting control (Ctrl) siRNA were purchased from Dharmacon (GE Healthcare). Transfections were performed using the siRNA transfection reagent INTERFERin (Polyplus transfection) following the manufacturer's instructions. Briefly, 0.1 mL of serum-free

media-containing 50 nM siRNA duplexes and INTERFERin was added to cells contained in clear polystyrene 24-well culture plates. To obtain cells with undetectable levels of CD147 protein, cells required a 96 h incubation period following the siRNA treatment.

Cell culture transfections

All DNA transfections of cultured cells were performed using jetPEI or jetPRIME transfection reagents (Polyplus Transfection) and carried out according to the manufacturer's instructions. Briefly, cells were transfected (3 µL reagent and 1.5 µg plasmid DNA per well [6-well plate]) and then incubated at 37 °C for 4 h. Following the 4 h incubation, media in the wells was replaced and the cells were incubated for 24 h at 37 °C to allow for expression of the respective gene product. Transfected cells were fixed (3% paraformaldehyde) for viewing by immunofluorescence microscopy.

Listeria monocytogenes invasion assay (microscopy counts)

CD147 was knocked-down in HeLa cells (in 24-well plates) using siRNA. 96 h post-incubation with CD147 (or non-targeting [control]) siRNA duplexes, cells were infected with wild-type *L. monocytogenes*. *L. monocytogenes* infections were rinsed 5× after 2 h using pre-warmed PBS [+/+] and then 1 mL of pre-warmed DMEM containing 10% FBS and gentamicin (50 µg/mL) was added to each infected well to kill any remaining extracellular bacteria. Cells were fixed 3 h post-infection. To label extracellular bacteria, samples were treated with rabbit anti-*Listeria monocytogenes* and Alexa Fluor 488-conjugated goat anti-rabbit antibodies as described above except Tween-20 was absent from all treatments. On the same day, samples were washed and permeabilized as described above. To label all bacteria (intracellular and extracellular), samples were treated with rabbit anti-*Listeria monocytogenes,* Alexa Fluor 594-conjugated goat anti-rabbit, mouse anti-CD147, and Alexa Fluor 350-conjugated goat anti-mouse antibodies (Tween-20 present). Samples were mounted onto glass microscope slides using the Prolong Diamond antifade mounting medium (without DAPI). When imaging samples, intracellular bacteria possessed signal solely from the Alexa Fluor 594-conjugated goat anti-rabbit antibodies, whereas extracellular bacteria were indicated by signal from both the Alexa Fluor 594- and the Alexa Fluor 488-conjugated goat anti-rabbit antibodies.

Listeria monocytogenes and *Shigella flexneri* intercellular spreading assays

CD147 was knocked-down in HeLa cells (in 24 well plates) using siRNA. 96 h post-incubation with CD147 (or non-targeting [control]) siRNA duplexes, cells were infected with wild-type *L. monocytogenes* or *S. flexneri*. *L. monocytogenes* infections were rinsed 5× after 2 h using pre-warmed PBS [-/-], and then, 1 mL of pre-warmed DMEM containing 10% FBS and gentamicin (50 µg/mL) was added to each infected well to kill any remaining extracellular bacteria. Culture plates infected with *S. flexneri* infections were washed after 1 h as describe above. After 8 h of infection, cells were fixed and permeabilized using warm (37 °C) 3% paraformaldehyde and 0.2% triton X-100 (as described above). Bacteria were detected with rabbit anti-*Listeria monocytogenes* or rabbit anti-*Shigella flexneri* antisera followed by secondary antibody labelling with Alexa Fluor 594-conjugated goat anti-rabbit antibodies. Infection foci (imaged at 400× magnification) and spreading area determination was performed as described by Talman and co-workers [20]. To determine the number of infected host cells per infection focus, host cells infected with bacteria were enumerated (infection of a host cell was scored visually by the microscopist). This was accomplished using a combination of (1) examining bacterially derived actin-rich structures (actin clouds, comet/rocket tails, and membrane protrusions) generated by the bacteria within the host cells and (2) general visual detection of the host cell as well as bacteria using nuclear staining (DAPI). A host cell was scored as infected by the microscopist if at least one actin cloud, comet/rocket tail, or membrane protrusion was evident within the cytoplasm of the host cell or if a bacterially generated membrane protrusion clearly extended laterally from the edge of the host cell.

Microscopy

Images were acquired using a Leica DMI4000B (Leica Microsystems) inverted fluorescent microscope fitted with a Hamamatsu Orca R2 CCD camera (Hamamatsu Photonics). All devices were controlled by MetaMorph Imaging System software (Universal Imaging). Images acquired were evaluated and processed using Metamorph Imaging System software or ImageJ.

Listeria monocytogenes comet/rocket tail and membrane protrusion analysis

L. monocytogenes comet/rocket tail lengths were measured manually using the line tool in the ImageJ software. Measurement was taken from cells infected for 8 h. Any comet/rocket tails which were not visually in focus within 5 z slices (height of 0.8 µm) were excluded from measurements as were those where a clear beginning (bacterium–tail interface) and end could not be ascertained. Membrane protrusion lengths were measured as described by the above criteria. In addition, only membrane protrusions that extended

outwards from the edges of the host cell (in the x–y-plane) were included in measurements and not those which protruded upwards (in the z-plane) and were not at the edges of the cell. To determine the distortedness of comet/rocket tails and membrane protrusions, we calculated the tortuosity index of the structures which is defined as the ratio of the actual tail/membrane protrusion length to the shortest distance between the bacterium–tail interface and the end of the tail/membrane protrusion [5].

Western blot quantification

Protein quantification was performed using the gels tool in ImageJ. For each independent blot, all analyzed lanes were first adjusted for loading by normalizing the loading control signal against one of the control lanes. Following this, CD147 signal in all lanes was normalized against one of the control lanes. To obtain the adjusted and relative CD147 protein levels of each lane, the relative CD147 signal of each lane was divided by the relative loading control of that same lane.

Statistical analysis

Statistical analysis was performed (unblinded) using GraphPad Prism version 6.01. All results involving immunofluorescence microscopy and Western blotting were obtained from experiments performed at least three times ($n = 3$) unless otherwise stated. Measurements were normalized to controls where indicated. All images shown are representative of experiments performed.

Results

CD147 is recruited to *L. monocytogenes* actin-rich membrane protrusions and corresponding invaginations

To investigate the potential involvement of CD147 during the intracellular motility and cell-to-cell spreading of *L. monocytogenes*, we immunolocalized CD147 in HeLa cells infected with wild-type *L. monocytogenes*. Immunostaining of these cells revealed CD147 at the plasma membrane surrounding *L. monocytogenes* membrane protrusions as well as particularly intense CD147 localization as clusters at the plasma membrane where motile bacteria had just begun to protrude outwards from the host cell (Fig. 1a, b). Staining was not present within the actin-rich core of the membrane protrusions or at cytoplasmic comet/rocket tails (Fig. 1a, b). Primary antibody controls using normal mouse IgG in place of the anti-CD147 antibody did not concentrate at those sites. (Fig. S1A). To ensure that an abnormal accumulation of the plasma membrane itself was not the cause of the observed increase in CD147 localization, we transfected cells with a fluorescent plasma membrane marker (pmKate2-f-mem) and then infected the cells with *L. monocytogenes*. In those cells, we noticed that while the plasma membrane marker delineated the membrane at the *L. monocytogenes* protrusions, it did not increase, as was the case at other actin-rich membranous structures (membrane ruffles or filopodial extensions) (Fig. S1c). To test whether the presence of CD147 at *L. monocytogenes* membrane protrusions was applicable in other cell types or was a cell-type specific observation, we infected human intestinal epithelial (Caco-2) cells with *L. monocytogenes* and stained fixed samples with anti-CD147 antibodies. CD147 was again enriched at the plasma membrane at sites of bacterial spreading from one cell to another (Fig. S2).

Because CD147 is a transmembrane receptor that homotypically associates with CD147 molecules on neighboring cells [21], we examined whether CD147 was concentrated at the corresponding plasma membrane of invaginations at sites of *L. monocytogenes* membrane protrusion contact. To do this, we infected wild-type cells with *L. monocytogenes* and then mixed them with GFP-CD147 transfected cells and observed GFP-CD147 surrounding *L. monocytogenes*-containing invaginations in the GFP-CD147-positive membrane protrusion receiving cells (Fig. 1c-top). GFP-CD147 was also enriched at the plasma membrane surrounding the membrane protrusions generated from GFP-CD147 cells when we performed the reverse experiments (Fig. 1c-bottom). As a control, we performed the same experiments using the GFP empty vector in place of GFP-CD147, and saw that GFP on its own was not present at *L. monocytogenes* membrane protrusions or their corresponding invaginations (Fig. S1b). Upon the interaction of *L. monocytogenes* membrane protrusions with the corresponding invaginations of neighboring cells, we noticed a dramatic increase in endogenous CD147 signal (detected by antibody staining). We presume that this was due to the localization of proteins from both the membrane protrusion and invagination fluorescing in the same localized area (Fig. 1d). We examined similar contact sites using normal mouse IgG in place of the anti-CD147 antibody and did not see a concentration of the signal at those sites (Fig. S1a).

We then determined the frequency of endogenous CD147 redistribution at *L. monocytogenes* membrane protrusions and saw that there was an increase in CD147 fluorescence intensity at ~ 99% of the structures (68 membrane protrusions quantified over three independent experiments) (Fig. 1e). When we quantified the frequency of increased GFP-CD147 signal at corresponding invaginations, we saw that 100% of the structures were enriched with GFP-CD147 (37 membrane protrusion invaginations quantified over three independent experiments) (Fig. 1f).

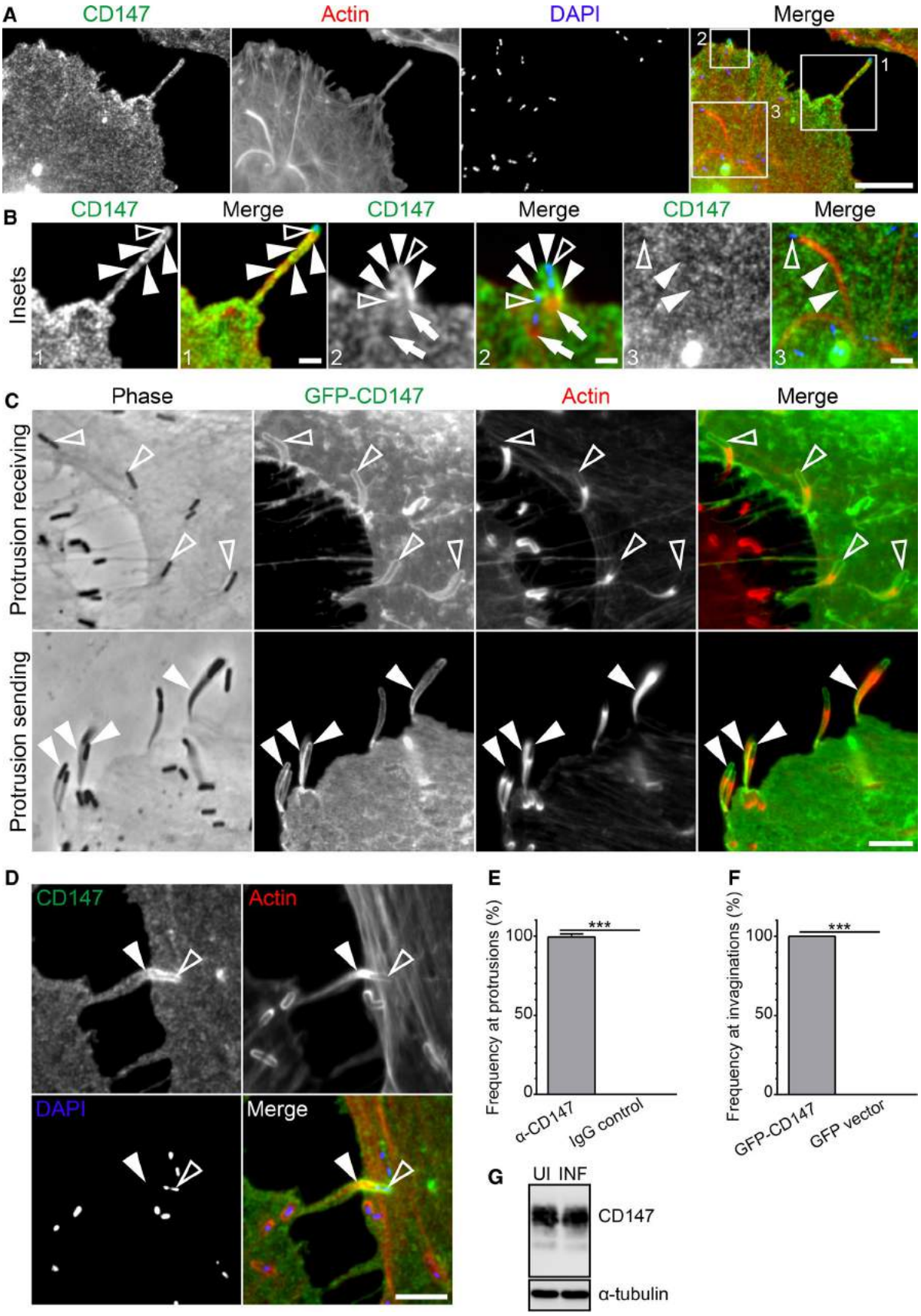
A
CD147
Actin
DAPI
Merge
B
Insets
CD147
Merge
C
Phase
GFP-CD147
Protrusion receiving
Protrusion sending
D
E
Frequency at protrusions (%)
α-CD147
IgG control
F
Frequency at invaginations (%)
GFP-CD147
GFP vector
G
UI INF
α-tubulin

◂**Fig. 1** CD147 is recruited to the plasma membrane of *L. monocytogenes* actin-rich membrane protrusions and corresponding invaginations. **a** HeLa cells infected with wild-type *L. monocytogenes* for 6 h (comet/rocket tail and membrane protrusion formation) were fixed and then stained with a mouse monoclonal CD147 targeting antibody (green), Alexa594-phalloidin (red) to visualize F-actin, and DAPI (blue) to visualize DNA. CD147 is enriched at the plasma membrane surrounding membrane protrusions but not at actin clouds or comet/rocket tails. Boxed regions indicate the following bacterially generated structures: (1) an extended membrane protrusion, (2) early stage of membrane protrusion formation, and (3) cytosolic comet/rocket tails. Scale bar is 10 µm. **b** Enlargements of boxed regions from **a**. Open arrowheads indicate the location of *L. monocytogenes* bacteria. Solid arrowheads point to the following structures: extended membrane protrusion (1), plasma membrane surrounding early membrane protrusion (2), and cytosolic comet/rocket tails (3). Full arrow in box 2 indicates the location of actin-rich cytosolic comet/rocket tails. Scale bars are 2 µm (box 1 and box 3) and 1 µm (box 2). **c** HeLa cells were transfected with GFP-CD147. GFP-CD147 is present at *L. monocytogenes* membrane protrusions originating from GFP-CD147-positive HeLa cells (sending cell) as well as at corresponding membrane invaginations when GFP-CD147 is expressed in protrusion receiving cells. Solid arrowheads point to GFP-CD147 at extended *L. monocytogenes* membrane protrusions and open arrowheads indicate GFP-CD147 at invaginations. Scale bar is 5 µm. **d** Endogenous CD147 signal at *L. monocytogenes* membrane protrusions is intensified when the structures are engulfed by invaginations formed in neighboring (receiving) cells. The open arrowhead indicates the location of a *L. monocytogenes* bacterium. The solid arrowhead points to the invading *L. monocytogenes* membrane protrusion. Scale bar is 5 µm. Percent frequency of CD147 enrichment at *L. monocytogenes* membrane protrusions (**e**) and invaginations (**f**). Results are presented as a bar graph of the average percent frequency (± standard deviation [SD]). 89 *L. monocytogenes* membrane protrusions (for each antibody and from ten microscopy field of views, [**e**]) and 37 *L. monocytogenes* membrane protrusion invaginations (for each DNA construct and from ten microscopy field of views, [**f**]) were analyzed. The average percent value of CD147 enrichment is as follows: 99% [α-CD147] vs 0% [IgG control] (**e**) and 100% [GFP-CD147] vs 0% [GFP vector] (**f**). ***$p < 0.0001$ (unpaired Mann–Whitney *U* test). **g** Western blot of uninfected (UI) and 8 h *L. monocytogenes* infected (INF) HeLa whole-cell lysate probed with a mouse monoclonal anti-CD147 antibody shows no alteration in CD147 protein levels. The blot was stripped and re-probed with a mouse anti-α-tubulin antibody to confirm equal loading

The altered localization of CD147 in infected cells did not result in a change in protein levels when compared to uninfected cells (Fig. 1g). We also performed infections using an *L. monocytogenes actA*-deletion mutant, which is unable to generate F-actin networks at its surface and is, thus, non-motile. We found that CD147 did not recruit to the vicinity of those bacteria (Fig. S3).

CD147 is required for the proper formation of *L. monocytogenes* actin-rich membrane protrusions

To determine the functional role of CD147 at bacterially induced actin-rich structures generated during *L. monocytogenes* infections, we depleted CD147 in HeLa cells using siRNA (Fig. S4A). Western blot analysis of depleted cells resulted in a ~ 90% reduction in CD147 protein levels when compared to cells treated with non-targeting [control] siRNA (Fig. S4b). Till and colleagues [22] previously demonstrated that CD147 was used by *L. monocytogenes* for efficient internalization into HEK293 (kidney epithelial) cells. Depletion of CD147 within those cells caused a ~ twofold decrease in intracellular bacterial loads [22]. Here, we examined whether a similar invasion defect would arise in siRNA-treated HeLa cells. We utilized immunofluorescence microscopy to quantify *L. monocytogenes* invasion by enumerating the proportion of intracellular bacteria versus total bacteria (extracellular and intracellular) contained within host cells that had undetectable levels of CD147. We found a ~ 50% reduction in the levels of internalized bacteria in cells depleted of CD147 as compared to cells treated with non-targeting [control] siRNA (Fig. 2a). As CD147 was absent from comet/rocket tails (Fig. 1a3, b3), it was not surprising that the comet/rocket tails appeared indistinguishable between CD147 depleted cells and cells treated with non-targeting [control] siRNA (Fig. S4c). To examine comet/rocket tails in more detail, we examined the lengths and tortuosity (a measure of comet/rocket tail distortedness) of the structures generated in cells treated with CD147-targeting or with non-targeting [control] siRNA. In both treatments, we found no significant differences in the length or tortuosity of comet/rocket tails generated in cells that expressed wild-type or depleted levels of CD147 (Fig. 2b, c). In addition, we saw no significant shifts to the proportions of short (< 5 µm), medium (5 to < 10 µm and 10 to < 15 µm), and long (15 µm) comet/rocket tails (Fig. 2d).

CD147 depletion in *L. monocytogenes* infected cells resulted in morphologically deformed membrane protrusions when compared to their counterparts in cells treated with non-targeting [control] siRNA (Fig. 2e, f). The morphologically altered membrane protrusions resembled those generated in CypA-/- cells [8]. Similar CD147 localization patterns and phenotypic alterations to *L. monocytogenes* membrane protrusions were observed during immunolocalization and siRNA experiments conducted in SKOV3 and A549 cell lines (Fig. S5a, b). Because these structures are crucial in allowing *L. monocytogenes* to spread amongst host cells, we studied, in greater detail, the effect that CD147 depletion had on their length and tortuosity. When we measured the length of membrane protrusions, we found that depletion of CD147 resulted in significantly shorter structures (Fig. 2g). We also noted a significant increase in the tortuosity of membrane protrusions as they were severely contorted in CD147-depleted cells compared to their straighter counterparts in control cells (Fig. 2h, i). In cells depleted of CD147, *L. monocytogenes* membrane protrusions became more distorted as they became longer (Fig. 2j).

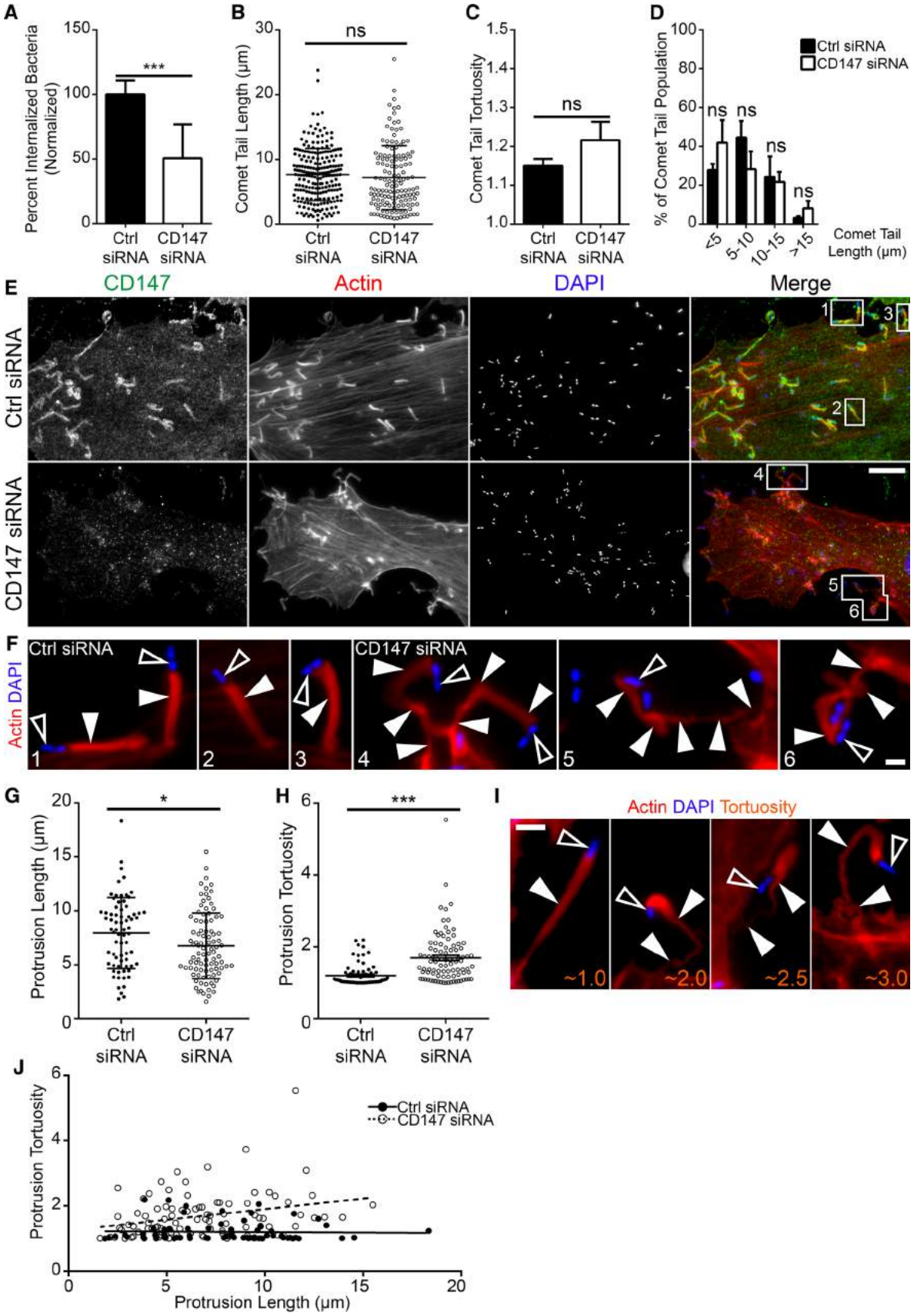
A
Percent Internalized Bacteria (Normalized)
150
100
50
0
***
Ctrl siRNA
CD147 siRNA
B
Comet Tail Length (μm)
30
20
10
0
ns
Ctrl siRNA
CD147 siRNA
C
Comet Tail Tortuosity
1.5
1.4
1.3
1.2
1.1
1.0
ns
Ctrl siRNA
CD147 siRNA
D
% of Comet Tail Population
100
80
60
40
20
0
Ctrl siRNA
CD147 siRNA
ns
ns
ns
ns
<5
5-10
10-15
>15
Comet Tail Length (μm)
E
CD147
Actin
DAPI
Merge
Ctrl siRNA
CD147 siRNA
1
2
3
4
5
6
F
Actin DAPI
Ctrl siRNA
CD147 siRNA
1
2
3
4
5
6
G
Protrusion Length (μm)
20
15
10
5
0
*
Ctrl siRNA
CD147 siRNA
H
Protrusion Tortuosity
6
4
2
0
***
Ctrl siRNA
CD147 siRNA
I
Actin DAPI Tortuosity
~1.0
~2.0
~2.5
~3.0
J
Protrusion Tortuosity
6
4
2
0
Ctrl siRNA
CD147 siRNA
0
5
10
15
20
Protrusion Length (μm)

◂**Fig. 2** CD147 is crucial for the proper formation of *L. monocytogenes* actin-rich membrane protrusions. **a** Quantification of *L. monocytogenes* internalization into cells treated with non-targeting [control] (Ctrl siRNA) or CD147-targeting (CD147 siRNA) siRNA duplexes. 39 non-targeting [control] and 24 CD147-targeting siRNA-treated HeLa cells infected with *L. monocytogenes* were examined. The total number of bacteria counted (inside and out) were 3259 (Ctrl siRNA) and 597 (CD147 siRNA). The percentage of internalized bacteria (relative to control, ± SD) is 100% (Ctrl siRNA) and 51% (CD147 siRNA). ***$p < 0.0001$ (unpaired parametric two-tailed *t* tests [with Welch's correction]). Quantification of *L. monocytogenes* comet/rocket tail lengths (**b**) and tortuosity (**c**) in non-targeting [control] (Ctrl siRNA) and CD147-targeting (CD147 siRNA) siRNA-treated HeLa cells. 220 comet/rocket tails (from 18 microscopy field of views) were measured from cells treated with non-targeting [control] siRNA. 138 comet/rocket tails (from 14 microscopy field of views) were measured from cells treated with CD147-targeting siRNA. The average comet/rocket tail lengths (depicted as a scatter plot, ± SD) are 7.666 µm in Ctrl siRNA-treated cells and 7.167 µm in CD147 siRNA-treated cells. The average comet/rocket tail tortuosities (± standard error of mean [s.e.m.]) are 1.150 in Ctrl siRNA-treated cells and 1.216 in CD147 siRNA-treated cells. **d** Results from (**b**) were plotted as binned (< 5, 5 to < 10, 10 to < 15, and > 15 µm) comet/rocket tail lengths. The percent distribution of comet/rocket tail lengths (± SD) are < 5 µm (28% Ctrl siRNA and 42% CD147 siRNA; not significant [ns]), 5 to < 10 µm (45% Ctrl siRNA and 28% CD147 siRNA; ns), 10 to < 15 µm (24% Ctrl siRNA and 22% CD147 siRNA; ns), and > 15 µm (3% Ctrl siRNA and 8% CD147 siRNA; ns). **e** HeLa cells were treated with non-targeting [control] (Ctrl siRNA) or CD147-targeting (CD147 siRNA) siRNA duplexes and infected with wild-type *L. monocytogenes* for 6 h. Cells were fixed and stained with a mouse anti-CD147 monoclonal antibody (green), DAPI (blue) to visualize DNA, and Alexa 594-phalloidin (red) to visualize F-actin. CD147 is abundant at the morphologically normal actin-rich *L. monocytogenes* membrane protrusions (Ctrl siRNA). *L. monocytogenes* membrane protrusions generated in CD147 depleted cells (CD147 siRNA) are highly contorted. Scale bar is 10 µm. **f** Enlargement of *L. monocytogenes* membrane protrusions from numbered boxed regions in (**e**). Open arrowheads indicate *L. monocytogenes* bacteria (blue), while solid arrowheads point to the corresponding membrane protrusions (red). Color intensities were enhanced from (**e**) to clearly identify the bacteria and membrane protrusions. Scale bar is 1 µm. Quantification of *L. monocytogenes* membrane protrusion lengths (**g**) and tortuosity (**h**) in non-targeting [control] (Ctrl siRNA) and CD147-targeting (CD147 siRNA) siRNA-treated HeLa cells. 71 membrane protrusions (from 36 microscopy field of views) were measured from cells treated with non-targeting [control] siRNA. 93 membrane protrusions (from 34 microscopy field of views) were measured from cells treated with CD147-targeting siRNA. The average membrane protrusion lengths (± SD) are 7.942 µm in Ctrl siRNA-treated cells and 6.764 µm in CD147 siRNA-treated cells. The average membrane protrusion tortuosities (± SEM) are 1.204 in Ctrl siRNA-treated cells and 1.692 in CD147 siRNA-treated cells. **$p < 0.05$ (unpaired parametric two-tailed *t* tests [with Welch's correction], $n = 4$, **g**); ***$p < 0.0001$ (unpaired Mann–Whitney *U* test, $n = 4$, **h**). **i** Representative immunofluorescent images of various membrane protrusion tortuosities (orange). Alexa 594-phalloidin (red) was used to visualize the membrane protrusion (solid arrowheads) and DAPI (blue) to indicate *L. monocytogenes* bacteria (open arrowheads). Scale bar is 2 µm. **j** Data from (**g** and **h**) were plotted as an XY graph with linear regression lines (lines ($Y = -0.003069 \times X + 1.228$ [Ctrl siRNA] and $Y = 0.06493 \times X + 1.253$ [CD147 siRNA]; slopes are significantly different)

We previously showed that misshaped *L. monocytogenes* membrane protrusions generated in CypA knock-out (KO) cells retained the membrane-cytoskeletal linker ezrin within the actin-rich core of the structures [8]. Thus, we looked for the presence of endogenous ezrin at the deformed *L. monocytogenes* membrane protrusions generated in cells that were treated with CD147-targeting siRNA. Again, we saw that ezrin was present at high levels at the structures (Fig. S6a–c) as well as at morphologically sound membrane protrusions generated in cells treated with non-targeting [control] siRNA (Fig. S6a, b).

Our observation that CD147 depletion phenocopies the resulting contorted membrane protrusions generated in CypA KO cells [8] prompted us to investigate the distribution of the two proteins at the structures. We initially examined the progression of endogenous CD147 together with CypA from the initiation of membrane protrusion formation to maturity to determine whether the proteins colocalized to the same regions at the membrane protrusions. At the earliest stage of protrusion formation where the bacterium has just contacted the host cell plasma membrane, CD147 was found at one pole of the bacterium, whereas CypA was present as a single intense zone at the opposite pole of *L. monocytogenes*, adjacent to the host cell cytoplasm (Fig. S7, box 1). Increased presence of both proteins continued with CD147 enriched around the entire top of the bacterial cell at regions where the host cell plasma membrane envelops the bacterium, while CypA was enriched at the opposite pole of the bacterium where the actin-rich comet/rocket tail originates (Fig. S7, box 2). Once the actin comet/rocket tail had pushed the bacterium outwards causing the plasma membrane to protrude further, CypA localized within the actin-rich core of the structure, while CD147 continued to be recruited around the entire membrane of the *L. monocytogenes* protrusion (Fig. S7, box 3). This localization continued until the point where the membrane protrusion extended far from the host cell body (Fig. S7, boxes 4–6). Although some signal mixing could be detected at the actin-core/plasma membrane interface (yellow signal), intermixing of the two signals was prominent at zones where the structures narrowed (Fig. S7, boxes 5, 6).

Next, we wanted to investigate regions of CD147 that could be involved with (1) the stabilization of *L. monocytogenes* membrane protrusions and (2) the potential recruitment of CypA to the structures. To do this, we treated infected cells with a CD147 blocking antibody (called MEM-M6/1) that targets the N-terminal Ig domain of the protein [23, 24]. We added the CD147 blocking antibody (vs normal mouse IgG [control]) to wild-type host cells 2 h post-infection and allowed the infections to proceed for an additional 5 h to observe membrane protrusions. In samples treated with the CD147 blocking antibody, collapsed membrane protrusions that failed to extend outward from

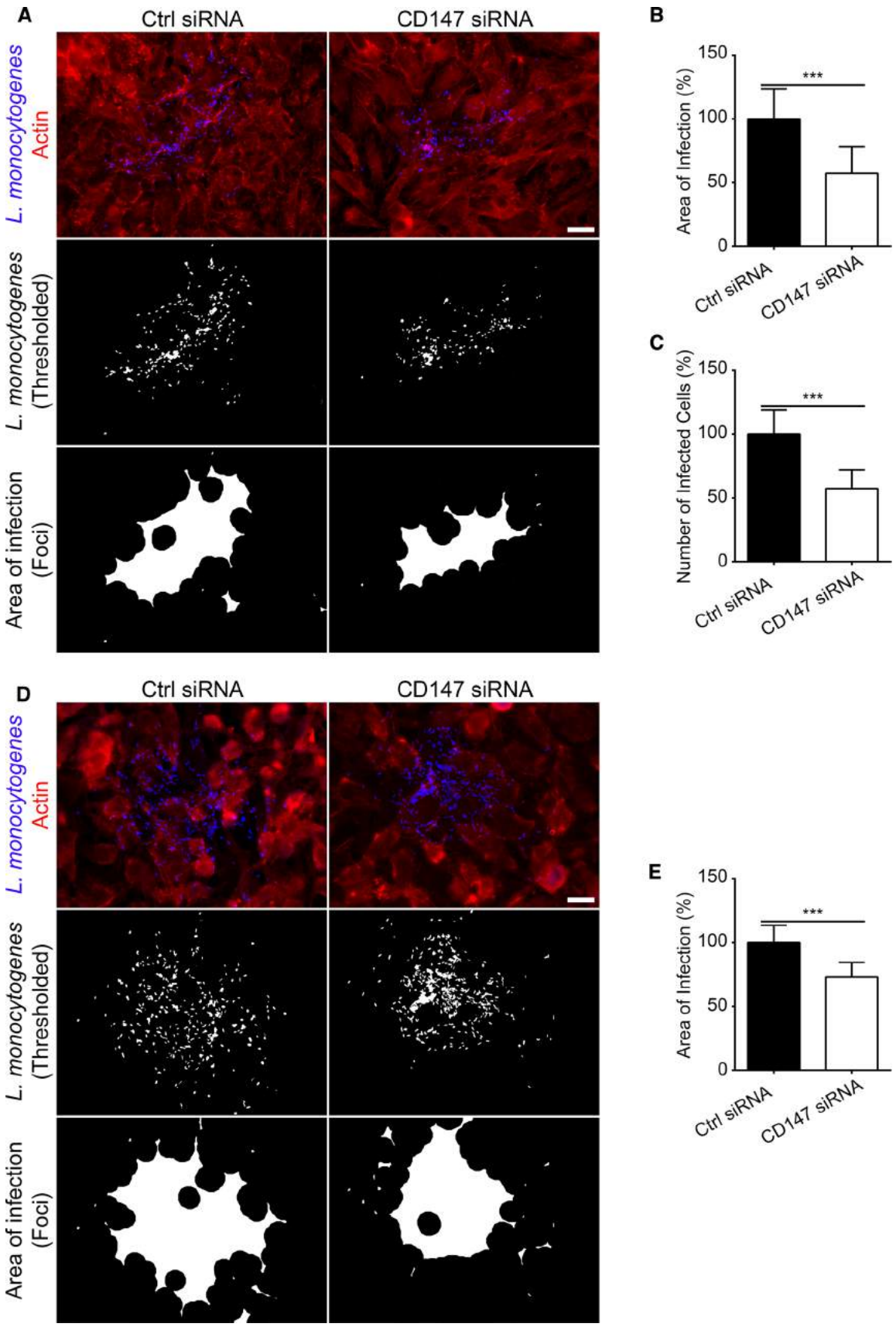
A
Ctrl siRNA
CD147 siRNA
L. monocytogenes
Actin
L. monocytogenes
(Thresholded)
Area of infection
(Foci)
B
Area of Infection (%)
150
100
50
0
***
Ctrl siRNA
CD147 siRNA
C
Number of Infected Cells (%)
150
100
50
0
***
Ctrl siRNA
CD147 siRNA
D
Ctrl siRNA
CD147 siRNA
L. monocytogenes
Actin
L. monocytogenes
(Thresholded)
Area of infection
(Foci)
E
Area of Infection (%)
150
100
50
0
***
Ctrl siRNA
CD147 siRNA

◂**Fig. 3** CD147 promotes efficient *L. monocytogenes* cell-to-cell spreading. **a** Images of 8 h *L. monocytogenes* infection foci from HeLa cells treated with non-targeting [control] (Ctrl siRNA) or CD147-targeting (CD147 siRNA) siRNA sequences. Cells were fixed and stained with a mouse anti-CD147 monoclonal antibody (see Fig. S7), rabbit anti-*Listeria monocytogenes* polyclonal antibody (blue) and Alexa 594-phalloidin (red) to visualize F-actin (top). *L. monocytogenes* bacteria only (middle) and delineated infection foci (bottom). Scale bar is 20 µm. Quantification of infection foci area and number of infected cells contained within foci from HeLa cells treated with non-targeting [control] (Ctrl siRNA) or CD147-targeting (CD147 siRNA) siRNA sequences. At least 40 infection foci (54 foci from cells treated with non-targeting [control] siRNA and 40 foci from cells treated with CD147-targeting siRNA) were imaged and analyzed. Percent values (relative to control, [± SD]) are 100% [Ctrl siRNA] and 57% [CD147 siRNA] in (**b**) and 100% [Ctrl siRNA] and 57% [CD147 siRNA] in (**c**). ***$p < 0.0001$ (unpaired parametric two-tailed *t* tests [with Welch's correction]. **d** Images of 8 h *L. monocytogenes* infection foci from SKOV3 cells treated with non-targeting [control] (Ctrl siRNA) or CD147-targeting (CD147 siRNA) siRNA sequences. Cells were fixed and stained with a mouse anti-CD147 monoclonal antibody, rabbit anti-*Listeria monocytogenes* polyclonal antibody (blue) and Alexa 594-phalloidin (red) to visualize F-actin (top). *L. monocytogenes* bacteria only (middle) and delineated infection foci (bottom). Scale bar is 20 µm. **e** Quantification of infection foci area from SKOV3 cells treated with non-targeting [control] (Ctrl siRNA) or CD147-targeting (CD147 siRNA) siRNA sequences. 15 foci each from cells treated with non-targeting [control] and CD147-targeting siRNA were imaged and analyzed. Percent values (relative to control, [± SD]) are 100% [Ctrl siRNA] and 73% [CD147 siRNA]. ***$p < 0.0001$ (unpaired parametric two-tailed *t* tests [with Welch's correction]

the cell were evident, whereas samples treated with normal mouse IgG had membrane protrusions that appeared indistinguishable from wild-type protrusions (Fig. S8a, b). When we performed immunostaining of the CD147 antibody blocked samples against CD147 or CypA, both proteins were recruited to the membrane protrusions (Fig. S8a, b). To study any potential CD147-CypA interactions that might be at play within membrane protrusions, we transfected cells with a fluorescently tagged variant of CD147 mutated at its extracellular/membrane CypA-binding site (GFP-CD147-P211A) [19]. We found that this mutant of CD147 continued to localize to membrane protrusions and to the corresponding invaginations similarly to cells expressing wild-type GFP-CD147 (Fig. S9a). Filamentous actin and CypA localization also appeared unchanged at *L. monocytogenes* membrane protrusions in the GFP-CD147-P211A expressing cells (Fig. S9a, b). These data are consistent with our observation that depletion of either CD147 or CypA results in the opposing protein maintaining its presence within the structures (Fig. S9c, d).

Recent findings by Maïssa and colleagues uncover a novel actin-associated role for CD147 in organizing actin-rich membrane protrusions generated during *N. meningitidis* infections [16]. The authors identified a crucial protrusion stabilizing function of CD147 that is dependent on the interaction between the cytoplasmic tail of CD147 and the cytosolic actin-crosslinking and bundling protein α-actinin 4. Because membrane protrusions generated by *N. meningitidis* and *L. monocytogenes* share similar characteristics, we set out to examine whether α-actinin 4 is also hijacked by *L. monocytogenes* at their membrane protrusions. Immunostaining of infected HeLa cells against α-actinin 4 revealed an enrichment of the protein within the actin-rich core of the structures (Fig. S10a). We also found that α-actinin 4 localized to actin clouds as well as throughout the comet/rocket tails (Fig. S10b).

CD147 promotes *L. monocytogenes* cell-to-cell spreading

The malformation of *L. monocytogenes* membrane protrusions suggests that CD147 likely influences the ability of the microbes to spread amongst neighboring cells. To test this, we adapted a previously developed assay that relies on the identification of *L. monocytogenes* foci of infection (bacteria immunolabeled using anti-*L. monocytogenes* antibodies) and post-analysis (thresholding and delineation) of these regions to measure the area of infection [20]. We measured at least 40 thresholded and delineated foci (containing all bacteria) from samples treated with CD147-targeting or non-targeting [control] siRNA. We ensured that foci imaged from depleted samples contained exclusively cells with undetectable levels of CD147 (Fig. S11). We calculated close to a 50% reduction (compared to controls) in the area of infection when CD147 was depleted in cells (Fig. 3a, b). Because of potential variability in the size of the host cells within the infection foci, we enumerated the number of infected cells per foci. Relative to samples treated with non-targeting [control] siRNA, there was a significant ~ 50% decrease in the number of infected cells per foci in the absence of CD147. This suggests that our previous observations of the foci area spreading defects are unlikely a result of abnormal changes in the physical size of infected host cells (Fig. 3c). We also examined *L. monocytogenes* cell-to-cell spreading using the SKOV3 cell line and saw a significant reduction in the area of infection when CD147 was depleted in those cells (Fig. 3d, e).

Shigella flexneri is another invasive bacterial pathogen that becomes motile within host cells using comet/rocket tails and ultimately spreads amongst cells through the generation of actin-rich membranous protrusions [25]. Despite the morphological and functional similarities between membrane protrusions generated by *L. monocytogenes* and *S. flexneri*, the extent of shared molecular constituents that make up both structures likely remains incomplete. Thus, to examine whether CD147 was also a component of *S. flexneri* membrane protrusions, we immunolocalized CD147 in HeLa cells infected with wild-type *S. flexneri.* Immunostaining of these samples showed a noticeable increase in CD147 intensity at the plasma membrane of the structures

(Fig. S12a). Cell-to-cell spreading assays showed a significant ~ 25% reduction in the average number of infected cells per foci when CD147 was depleted from cells (Fig. S12b), suggesting that CD147 is a host factor required by multiple pathogens that disseminate from one cell to another using actin-rich membrane protrusions.

Discussion

In this study, we demonstrate a new role for the transmembrane glycoprotein, CD147, as a crucial component in the cell-to-cell spreading machinery of both *L. monocytogenes* and *S. flexneri*.

Our findings demonstrate that collapsed membrane protrusions generated in cells depleted of CD147 phenocopy the loss of its classical binding partner CypA [8]. The alteration to either of these proteins results in morphological changes to the membrane protrusions as well as defects in the cell-to-cell transfer of the bacteria. Although defects in cell-to-cell spreading has also been seen with ezrin/CD44 studies [9], our finding that ezrin maintains its localization within *L. monocytogenes* membrane protrusions when CD147 is depleted suggests that ezrin/CD44 is acting independently of CD147 and CypA during bacterial dissemination.

In our analysis, we found that depletion of CD147 caused *L. monocytogenes* membrane protrusions to become significantly shorter and contorted. The same phenotypes occurred in our previous study when *L. monocytogenes* was used to infect CypA KO cells [8]. This is in contrast to other studies where cells transfected with truncated forms of CD44 or a constitutively inactive variant of ezrin caused the proximal regions of *L. monocytogenes* membrane protrusions to thicken, distort, and shorten considerably [9]. We did not find any evident morphological changes to *L. monocytogenes* membrane protrusions when CD147 (or CypA [8]) was overexpressed.

As we investigated CD147-CypA interactions more deeply during *L. monocytogenes* infections, many of our findings suggested that this protein pair is likely not interacting in their classical manner at the bacterial membrane protrusions. One would predict that if CypA was interacting with CD147, CypA would delineate the membrane protrusions similarly to the CD147 immunostaining pattern. However, this was not the case as our colocalization experiments showed that CD147 and CypA largely occupy different locations within the membrane protrusions; CypA is within the core of the structures, while CD147 is enriched at the surrounding plasma membrane. In addition, expression of CD147 containing a mutation in the CypA-binding site of CD147 did not affect the formation of membrane protrusions nor the recruitment of endogenous CypA to the structures. Our demonstration that CD147 or CypA maintained their localization at collapsed membrane protrusions when the opposing protein was depleted in cells supports this conclusion. Further support comes from our previous study that suggested extracellular CypA is incapable of restoring the normal morphology of collapsed membrane protrusions generated in CypA KO cells [8].

Although the depletion of either CD147 or CypA causes membrane protrusions to collapse in morphologically similar manners, there is a lack of published findings linking CD147 to CypA within the cytoplasm. Therefore, what could be going on? We postulate that one mechanism behind the CD147- and CypA-mediated morphological stabilization of *L. monocytogenes* membrane protrusions may involve both proteins interacting separately with the actin-crosslinking proteins within the structures. In fact, Maïssa and colleagues' study of *N. meningitidis* infections identified a novel link between CD147 and the actin cytoskeleton at *N. meningitidis* membrane protrusions [16]. The authors' use of an immunoprecipitation and nano-liquid chromatography tandem–mass spectrometry screen for CD147-binding partners identified several actin-binding and crosslinking proteins. Of the novel CD147-binding partners, α-actinin 4 was further investigated and shown to stabilize *N. meningitidis* membrane protrusions via its direct interaction with the cytoplasmic tail region of CD147. Our finding of α-actinin 4 within the core of *L. monocytogenes* membrane protrusions suggests a potentially similar mechanism to the one used during *N. meningitidis* infections whereby the cytosolic region of CD147 recruits α-actinin 4 to stabilize the actin filaments within the membrane protrusions. As CypA itself does not possess any known actin-binding motifs and its PPIase activity is dispensable during *L. monocytogenes* infections, its precise mechanistic role at membrane protrusions will require further investigation.

Given that there are some similarities in the overall deficiencies of *L. monocytogenes* membrane protrusions when either CD147 or ezrin/CD44 is altered, is it possible that these proteins interact at the structures? Evidence for this may lie in the involvement of CD147 at other actin-associated structures. Expression of CD147 in eukaryotic cells is involved in controlling the formation and proper functioning of actin-rich lamellipodia and invadopodia [12–15]. A crucial component of invadopodia formation involves lipid raft signalling. Grass and colleagues demonstrated a role for CD147 together with CD44 at those sites to promote proper invadopodia activity [26]. Consequently, a mechanism behind *L. monocytogenes* membrane protrusion formation/stabilization could involve CD147 working together with CD44 to ultimately regulate and organize F-actin within the structures, whether through ezrin, α-actinin 4, or other actin-associated components.

We found that the cell-to-cell transfer of *L. monocytogenes* amongst CD147 siRNA-treated cells was decreased

by ~ twofold. Significant decreases in intercellular spreading also held true when tested in multiple cell lines as well as when host cells were infected with *S. flexneri*. Although not enumerated, alterations in bacterial cell-to-cell spreading were qualitatively assessed by others when an inactive ezrin variant or CD44 domains were overexpressed in *L. monocytogenes* infected monolayers [9]. Pust and co-workers noted in their ezrin/CD44 work that *L. monocytogenes* could infect at the edges of those monolayers, but that "*Listeria* did not infect the cells in the centre of a cellular islet" [9]. Whether those observed results were, in fact, due to a perturbation in bacterial spreading or a decrease in the initial bacterial entry (invasion) is questionable as Jung and colleagues demonstrated a crucial role for CD44 and ezrin in the initial uptake of *L. monocytogenes* into non-phagocytic host cells [27]. Although our study and work done by others suggests that CD147 promotes efficient bacterial invasion into target host cells [20], our intercellular spreading assays were specifically designed to study the cell-to-cell spread of *L. monocytogenes* into their neighboring cells. Furthermore, while we focused primarily on the pathogenesis of *L. monocytogenes,* our observation of defective bacterial spreading using *S. flexneri* demonstrates that CD147 is a host protein accessed by multiple microbes during their disease processes [16, 28, 29].

A dearth of studies has failed to identify any proteins present on the invaginations that receive the *L. monocytogenes* membrane protrusions in neighboring cells. Thus, our discovery of CD147 concentrated on both the membrane protrusions and their corresponding invaginations was of particular interest. CD147 binds homotypically with CD147 molecules on neighboring cells [21]. We postulate that these interactions may serve to strengthen the efficiency of bacterial internalization ultimately through a pulling/endocytic event acting on the receiving cell in conjunction with the pushing forces transmitted by the actin comet/rocket tails of the protruding bacterial structures.

In summary, we have demonstrated that CD147 is critical for the proper formation and function of *L. monocytogenes* and *S. flexneri* membrane protrusions. The novel role that this transmembrane glycoprotein plays at these membrane protrusions (and the corresponding invaginations) could have broad applications to various motile membrane-associated actin-rich structures generated by cells as well as other disease-causing microbial pathogens.

Acknowledgements We thank Pascale Cossart for providing *L. monocytogenes* strains (EGD BUG 600 wild-type and Δ*actA* mutant), Calvin Roskelley for providing the SKOV3 cells, and Tatiana Pushkarsky for preparing the CD147 plasmids.

Author contributions ASD and JAG conceived the study. KTL provided results for Figs. S6a–c and CY provided results for Fig. S4b. ASD performed all other experiments. RHC and MB provided CypA and CD147 reagents as well as expertise. All authors analyzed the data and wrote the manuscript.

Funding This work was supported by operating grants from the Natural Sciences and Engineering Research Council of Canada (355316 and RGPIN-2018-05100 to JAG), as well as SFU Departmental Funds to JAG. ASD is an SFU Multi-year funding award recipient.

References

1. Hernandez-Milian A, Payeras-Cifre A (2014) What is new in listeriosis? Biomed Res Int. https://doi.org/10.1155/2014/358051
2. Tilney L, Portnoy D (1989) Actin filaments and the growth, movement, and spread of the intracellular bacterial parasite, *Listeria monocytogenes*. J Cell Biol 109:1597–1608
3. Gaillard JL, Berche P, Mounier J, Richard S, Sansonetti P (1987) In vitro model of penetration and intracellular growth of *Listeria monocytogenes* in the human enterocyte-like cell line Caco-2. Infect Immun 55:2822–2829
4. Welch MD, Rosenblatt J, Skoble J, Portnoy DA, Mitchison TJ (1998) Interaction of human Arp2/3 complex and the Listeria monocytogenes ActA protein in actin filament nucleation. Science 281:105–108
5. Dhanda AS, Vogl AW, Albraiki SE, Otey CA, Beck MR, Guttman JA (2018) Palladin compensates for the Arp2/3 complex and supports actin structures during *Listeria* infections. mBio 9:e02259-17
6. Southwick FS, Purich DL (1994) Arrest of Listeria movement in host cells by a bacterial ActA analogue: implications for actin-based motility. Proc Natl Acad Sci USA 91:5168–5172
7. Welch M, Iwamatsu A, Mitchison T (1997) Actin polymerization is induced by Arp 2/3 protein complex at the surface of *Listeria monocytogenes*. Nature 385:265–269
8. Dhanda AS, Lulic KT, Vogl AW, McGee MM, Chiu RH, Guttman JA (2018) *Listeria* membrane protrusion collapse: requirement of Cyclophilin A for *Listeria* cell-to-cell spreading. J Infect Dis. https://doi.org/10.1093/infdis/jiy255
9. Pust S, Morrison H, Wehland J, Sechi A, Herrlich P (2005) *Listeria monocytogenes* exploits ERM protein functions to efficiently spread from cell to cell. EMBO J 24:1287–1300
10. Yurchenko V, Zybarth G, O'Connor M, Dai WW, Franchin G, Hao T, Guo H, Hung HC, Toole B, Gallay P, Sherry B, Bukrinsky M (2002) Active site residues of cyclophilin A are crucial for its signaling activity via CD147. J Biol Chem 277:22959–22965
11. Qian AR, Zhang W, Cao JP, Yang PF, Gao X, Wang Z, Xu HY, Weng YY, Shang P (2008) Downregulation of CD147 expression alters cytoskeleton architecture and inhibits gelatinase production and SAPK pathway in human hepatocellular carcinoma cells. J Exp Clin Cancer Res 27:50
12. Liang Q, Han Q, Huang W, Nan G, Xu BQ, Jiang JL, Chen ZN (2014) HAb18G/CD147 regulates vinculin-mediated focal adhesion and cytoskeleton organization in cultured human hepatocellular carcinoma cells. PLoS One 9:e102496
13. Curtin KD, Meinertzhagen IA, Wyman RJ (2005) Basigin (EMMPRIN/CD147) interacts with integrin to affect cellular architecture. J Cell Sci 118:2649–2660
14. Zhao P, Zhang W, Wang SJ, Yu XL, Tang J, Huang W, Li Y, Cui HY, Guo YS, Tavernier J, Zhang SH, Jiang H, Chen ZN (2011) HAb18G/CD147 promotes cell motility by regulating annexin II-activated RhoA and Rac1 signaling pathways in hepatocellular carcinoma cells. Hepatology 54:2012–2024
15. Grass GD, Bratoeva M, Toole BP (2012) Regulation of invadopodia formation and activity by CD147. J Cell Sci 125:777–788

16. Maïssa N, Covarelli V, Janel S, Durel B, Simpson N, Bernard SC, Pardo-Lopez L, Bouzinba-Ségard H, Faure C, Scott MGH, Coureuil M, Morand PC, Lafont F, Nassif X, Marullo S, Bourdoulous S (2017) Strength of Neisseria meningitidis binding to endothelial cells requires highly-ordered CD147/β2-adrenoceptor clusters assembled by alpha-actinin-4. Nat Commun 8:15764
17. Sun S, Guo M, Zhang J, Ha A, Yokoyama K, Chiu R (2014) Cyclophilin A (CypA) interacts with NF-κB subunit, p65/RelA, and contributes to NF-κB activation signaling. PLoS One 9:e96211
18. Yurchenko V, Pushkarsky T, Li JH, Dai WW, Sherry B, Bukrinsky M (2005) Regulation of CD147 cell surface expression: involvement of the proline residue in the CD147 transmembrane domain. J Biol Chem 280:17013–17019
19. Pushkarsky T, Yurchenko V, Vanpouille C, Brichacek B, Vaisman I, Hatakeyama S, Nakayama KI, Sherry B, Bukrinsky MI (2005) Cell surface expression of CD147/EMMPRIN is regulated by cyclophilin 60. J Biol Chem 280:27866–27871
20. Talman AM, Chong R, Chia J, Svitkina T, Agaisse H (2014) Actin network disassembly powers dissemination of *Listeria monocytogenes*. J Cell Sci 127:240–249
21. Yurchenko V, Constant S, Eisenmesser E, Bukrinsky M (2010) Cyclophilin-CD147 interactions: a new target for anti-inflammatory therapeutics. Clin Exp Immunol 160:305–317
22. Till A, Rosenstiel P, Bräutigam K, Sina C, Jacobs G, Oberg HH, Seegert D, Chakraborty T, Schreiber S (2008) A role for membrane-bound CD147 in NOD2-mediated recognition of bacterial cytoinvasion. J Cell Sci 121:487–495
23. Baba M, Inoue M, Itoh K, Nishizawa Y (2008) Blocking CD147 induces cell death in cancer cells through impairment of glycolytic energy metabolism. Biochem Biophys Res Commun 374:111–116
24. Kim MY, Cho JY (2016) Molecular association of CD98, CD29, and CD147 critically mediates monocytic U937 cell adhesion. Korean J Physiol Pharmacol 20:515–523
25. Bernardini M, Mounier J, d'Hauteville H, Coquis-Rondon M, Sansonetti P (1989) Identification of icsA, a plasmid locus of Shigella flexneri that governs bacterial intra- and intercellular spread through interaction with F-actin. Proc Natl Acad Sci USA 86(10):3867–3871
26. Grass GD, Tolliver LB, Bratoeva M, Toole BP (2013) CD147, CD44, and the epidermal growth factor receptor (EGFR) signaling pathway cooperate to regulate breast epithelial cell invasiveness. J Biol Chem 288:26089–26104
27. Jung C, Matzke A, Neimann HH, Schwerk C, Tenenbaum T, Orian-Rousseau V (2009) Involvement of CD44v6 in InlB-dependent *Listeria* invasion. Mol Microbiol 72:1196–1207
28. Bernard S, Simpson N, Join-Lambert O, Federici C, Laran-Chich M-P, Maïssa N, Bouzinba-Ségard H, Morand P, Chretien F, Taouji S, Chevet E, Janel S, Lafont F, Coureuil M, Segura A, Niedergang F, Marullo S, Courand P-O, Nassif X, Bourdoulous S (2014) Pathogenic Neisseria meningitidis utilizes CD147 for vascular colonization. Nat Med 20:725–731
29. Vanarsdall A, Pritchard S, Wisner T, Liu J, Jardetzky T, Johnson D (2018) CD147 promotes entry of pentamer-expressing human cytomegalovirus into epithelial and endothelial cells. mBio. https://doi.org/10.1128/mbio.00781-18